Spatially variable response of Antarctica's ice sheets to orbital forcing during the Pliocene

Molly Patterson

patterso@binghamton.edu

Binghamton University, SUNY

Christiana Rosenberg

Binghamton University

Osamu Seki

Hokkaido University

Masanobu Yamamoto

Hokkaido University https://orcid.org/0000-0003-1312-825X

Oscar Romero

MARUM

Mei Nelissen

Marine Palynology and Paleoceanography, Department of Earth Sciences, University of Utrecht
https://orcid.org/0009-0002-6802-2495

Francesca Sangiorgi

Utrecht University https://orcid.org/0000-0003-4233-6154

Nick Golledge

VUW

Georgia Grant

GNS Science https://orcid.org/0000-0002-2615-9322

William Arnuk

Binghamton University https://orcid.org/0000-0002-4133-8935

Benjamin Keisling

University of Texas Institute of Geophysics https://orcid.org/0000-0002-2182-2025

Tim Naish

Victoria University of Wellington

Richard Levy

GNS Science https://orcid.org/0000-0002-8783-0167

Stephen Meyers

University of Wisconsin - Madison https://orcid.org/0000-0003-4422-720X

Nicholas Sullivan

University of Wisconsin-Madison https://orcid.org/0000-0003-2009-8992

Jeanine Ash
Department of Earth, Environmental and Planetary Sciences, Rice University
Denise Kulhanek
Christian-Albrechts-University of Kiel https://orcid.org/0000-0002-2156-6383
Brian Romans
Department of Geosciences, Virginia Tech https://orcid.org/0000-0002-3112-0326
Natalia Varela
University of Virginia https://orcid.org/0000-0002-9611-9393
Harold Jones
Department of Earth Sciences, Binghamton University
François Beny
University of Lille https://orcid.org/0000-0002-2322-4299
Imogene Browne
College of Marine Science, University of South Florida
Giuseppe Cortese
GNS Science https://orcid.org/0000-0003-1780-3371
Isabela Cordeiro de Sousa
Geotop Research Center in Earth System Dynamics and Département des sciences de la Terre et de l'atmosphère, Université du Québec à Montréal (UQAM) https://orcid.org/0000-0001-7285-3633
Justin Dodd
Northern Illinois University
Oliver Esper
Alfred-Wegener-Institut
Jenny Gales
School of Biological & Marine Sciences, University of Plymouth https://orcid.org/0000-0003-4402-5800
David Harwood
University of Nebraska-Lincoln https://orcid.org/0000-0002-9449-2127
Saki Ishino
Research Institute of Geology and Geoinformation, Geological Survey of Japan
Sookwan Kim
Korea Institute of Ocean Science and Technology https://orcid.org/0000-0001-9960-2295
Sunghan Kim
Korea Polar Research Institute
Jan Sverre Laberg
UiT the Arctic University of Norway https://orcid.org/0000-0003-3917-4895
R. Leckie
University of Massachusetts
J. Müller

Alfred Wegener Institute, Helmholtz Centre for Polar and Marine Research https://orcid.org/0000-0003-0724-4131

Amelia Shevenell

University of South Florida https://orcid.org/0000-0002-6457-6530

Shiv Singh

Polar Biology Lab National Centre for Antarctic and Ocean Research (NCAOR)

Saiko Sugisaki

Research Institute of Geology and Geoinformation, Geological Survey of Japan, National Institute of Advanced Science and Technology (AIST),

Tina van de Flierdt

Imperial College London https://orcid.org/0000-0001-7176-9755

Tim van Peer

University of Leicester https://orcid.org/0000-0003-3516-4198

Wenshen Xiao

Tongji University https://orcid.org/0000-0002-7240-2274

Laura De Santis

Geophysics Division Instituto Nazionale di Oceanografia e di Geofisica Sperimentale (OGS)

Robert McKay

Victoria University of Wellington https://orcid.org/0000-0002-5602-6985

Article

Keywords:

Posted Date: September 5th, 2024

DOI: https://doi.org/10.21203/rs.3.rs-4837964/v1

Additional Declarations: There is **NO** Competing Interest.

Spatially variable response of Antarctica's ice sheets to orbital forcing during the Pliocene.

M.O. Patterson[1], C. Rosenberg[1], O. Seki[2], M. Yamamoto[3], O.E. Romero[4,5], M. Nelissen[6], F. Sangiorgi[6], N.R. Golledge[7], G. Grant[8], W. D. Arnuk[1], B. Keisling[9], T. Naish[7], R. Levy[7,8], S. Meyers[10], N. Sullivan[10], J. Ash[11], Kulhanek[1,12,13], B.W. Romans[14], N. Varela Valenzuela[14,15], H. Jones[1], F. Beny[16], I. Browne[17], G. Cortese[8], I. Cordeiro de Sousa[18], J. P. Dodd[19], O. M. Esper[20], J. Gales[21], D. Harwood[22], S. Ishino[23], S. Kim[24], S. Kim[25], J. S. Laberg[26], R. M. Leckie[27], J. Müller[28], A. Shevenell[17], S. Singh[29,30], S. T. Sugisaki[23], T. van de Flierdt[31], T. van Peer[32,33], W. Xiao[34], L. De Santis[35], and R. McKay[7].

[1]Department of Earth Sciences, Binghamton University, Binghamton, NY, USA
[2]Institute of Low Temperature Science, Hokkaido University, Japan
[3]Environmental Earth Science, Hokkaido University, Japan
[4]MARUM-Center for Marine Environmental Sciences, University of Bremen, Germany
[5]Alfred Wegener Institute, Helmholtz Centre for Polar and Marine Research, Am Alten Hafen 26, 27568 Bremerhaven, Germany
[6]Marine Palynology and Paleoceanography, Department of Earth Sciences, University of Utrecht, The Netherlands
[7]Antarctic Research Centre, Victoria University of Wellington, Wellington, New Zealand
[8]GNS Science, Lower Hutt, New Zealand
[9]Jackson School of Geosciences, The University of Texas at Austin, TX, USA
[10]Department of Geoscience, University of Wisconsin-Madison, Madison, WI 53706, USA
[11]Department of Earth, Environmental and Planetary Sciences, Rice University, Houston, TX, USA
[12]International Ocean Discovery Program, Texas A&M University, TX, USA
[13]Institute of Geosciences, Christian-Albrechts-Universität zu Kiel, Kiel, Germany
[14]Department of Geosciences, Virginia Tech, Blacksburg, VA, USA
[15]Department of Environmental Sciences, University of Virginia, Charlottesville, VA, USA
[16]Laboratoire d'Océanologie et de Géosciences, UMR 8187 CNRS/Univ Lille/ULCO, 8 Cité scientifique, F-59655
[17]College of Marine Science, University of South Florida, St. Petersburg, FL, USA
[18]Geotop Research Center in Earth System Dynamics and Département des sciences de la Terre et de l'atmosphère, Université du Québec à Montréal (UQAM), C.P. 8888 Succursale Centre-Ville, Montréal, QC, H3C 3P8, Canada
[19]Department of Geology and Environmental Geosciences, Northern Illinois University, DeKalb, IL, USA.
[20]Helmholtz Centre for Polar and Marine Research, Alfred Wegener Institute, Bremerhaven, Germany
[21]School of Biological & Marine Sciences, University of Plymouth, UK
[22]Department of Earth and Atmospheric Sciences, University of Nebraska-Lincoln, Lincoln, NE 68588-0340, USA
[23]Research Institute of Geology and Geoinformation, Geological Survey of Japan, National Institute of Advanced Science and Technology (AIST), Tsukuba, Japan
[24]Ocean Climate Response & Ecosystem Research Department, Korea Institute of Ocean Science & Technology, Republic of Korea
[25]Division of Polar-Earth System Sciences, Korea Polar Research Institute, Republic of Korea
[26]Department of Geosciences, University of Tromsø – the Arctic University of Norway, Norway
[27]Department of Geosciences, University of Massachusetts Amherst, MA, USA
[28]Marine Geology, Alfred Wegener Institute, Bremerhaven, Germany
[29]Polar Biology Lab, National Centre for Antarctic and Ocean Research (NCAOR), India
[30]Department of Botany, Institute of Science, Banaras Hindu University, India
[31]Department of Earth Science and Engineering, Imperial College London, London, UK
[32]National Oceanography Centre Southampton, University of Southampton, Southampton, UK
[33]School of Geography, Geology and the Environment, University of Leicester, Leicester, UK
[34]State Key Laboratory of Marine Geology, Tongji University, China
[35]Geophysics Division, Istituto Nazionale di Oceanografia e di Geofisica Sperimentale, Trieste, Italy

Variations in Earth's orbit pace global ice-volume/sea-level changes, but the variability in the response for different sectors of the Antarctic Ice Sheet (AIS) to orbitally-forced climate change

remains unclear. We present geological records of iceberg-rafted debris (IBRD) and other proxies from locations adjacent to the West Antarctic Ice Sheet (WAIS) and East Antarctic Ice Sheet (EAIS) spanning ~3.3-2.3 Ma. Iceberg calving events from the WAIS recorded in Ross Sea sediment cores show a linear response to orbital forcing at timescales corresponding to obliquity (40 kyr) and precession (23-19 kyr) modulated by eccentricity (100 kyr). This contrasts with records adjacent to the EAIS, which lack obliquity pacing. Geological data and ice sheet model sensitivity tests show the WAIS is highly dynamic and responsive to oceanic melt driven by changes in Southern Ocean circulation, together with atmospheric forcing through variations in local insolation. Conversely, the EAIS appears less responsive to oceanic forcing, despite being the dominant source of meltwater to the global ocean during the mid-Pliocene. Our results imply a significant role for atmospheric warming on mid-Pliocene sea-level.

Paleoclimate reconstructions of the Pliocene provide insights into the response of Earth system components under climate forcing scenarios that are analogous to future projections[1]. Proxies developed from these records suggest that the mid-Pliocene (~3.26 to 3.0 Ma) was the last time atmospheric CO_2 levels exceeded 400 ppm[2,3,4–6] and global mean temperatures were >2°C above pre-industrial values and even warmer in polar regions[5,6]. Discontinuous ice-proximal drill core data indicate that marine-based portions of the WAIS advanced and retreated across the continental shelves at orbital periodicities[7], while ice sheet models[8] and paleoenvironmental data[9,10] show that WAIS variance was largely regulated by shifts in oceanic heat flux to the Antarctic continental margin. The deep ocean benthic $\delta^{18}O$ proxy, and far-field sea level records[11,12] provide continuous records of the pacing and magnitude of global ice volume changes, compared to the often discontinuous nature of ice-proximal and marginal records. While benthic $\delta^{18}O$ and sea level records are globally integrated signals, they lack the ability to determine if there exist spatially differences in how sectors of the AIS respond to different orbital frequencies, and thus mask potentially sensitivities of WAIS and EAIS margins to different kinds of environmental change predicted to provoke ice-sheet response in the future.

Here, we address how variations in orbitally-driven insolation manifest as climate and oceanic feedbacks to directly influence AIS mass balance at a catchment scale and the implications for global sea-level. Previous studies from the Antarctic margin have identified eccentricity (~400 and 100-kyr), obliquity (~41-kyr) and precession (~20-kyr) regulated AIS variance, and attributed these to temporal shifts in the dominant orbital frequencies to long-term secular variations in atmospheric CO_2 and Earth's mean climate state[7,10,13–16]. In this context, it has been hypothesised that marine ice sheets are inherently more sensitive to obliquity-paced forcing[7,10,15,17]. This is because changes in Earth's axial tilt strongly regulate mean annual insolation and the pole-equator temperature gradient, altering the zonal position of Southern Hemisphere westerly winds[e.g., 7]. When these wind fields are further south, the resultant upwelling brings relatively warmer Circumpolar Deep Water into contact with ice shelf cavities and marine-grounding lines[18–20] triggering marine ice sheet instabilities[e.g., 21,22] and a pronounced response to obliquity-driven ocean forcing. In contrast, variations in local insolation forcing primarily result from shifts in seasonal intensity and duration associated both with 400 and 100-kyr eccentricity-modulated precession (20 kyr) cycles, in addition to obliquity[e.g., 10,23]. However, long-term changes in local summer insolation can directly influence the general nature of glacial-interglacial AIS variability[e.g., 10]. When atmospheric warming thresholds are crossed, the sea ice that rings the Antarctic continent melts, allowing incursions of oceanic heat[e.g., 24] and atmospheric rivers[e.g., 25] to the AIS margin[10,15], thus driving surface melt of the ice sheet its fringing ice shelves, leading to enhanced iceberg calving through hydrofracturing of ice shelves and the creation of unstable ice-cliffs[22].

Here, we compare geological records from two different marine-based sectors of the AIS, the Ross Sea and Wilkes Land margins. Ice sheet model sensitivity tests suggest these two sectors have different thresholds for oceanic and atmospheric warming to trigger marine-ice sheet instabilities, with the entire WAIS (including the Ross Sea) and Recovery Basin region of EAIS being highly sensitive to oceanic warming even in the absence of atmospheric warming, whereas Wilkes Land and Aurora subglacial basins require atmospheric warming of >3°C for marine ice sheet loss to be triggered[30]. In

order to test this model result and determine if WAIS and EAIS responded the same or differently to orbital forcing in a similar-to-present (Pliocene) background climate, we compare a newly obtained, continuous mid- to Late Pliocene record of Iceberg Rafted Debris (IBRD) Mass Accumulation Rates (MAR) from Ross Sea International Ocean Discovery Program (IODP) Site U1524 adjacent to the WAIS margin with IODP Site U1361 offshore of the Wilkes subglacial basin adjacent to the EAIS[15] (Fig. 1). Modern iceberg trajectories demonstrate the source margins for icebergs across these two sites are distinct, despite their close proximity to one another (Fig. 1). Iceberg tracks are closely tied to surface ocean currents. Thus, the majority of icebergs in the Ross Sea sector are sourced from the WAIS and become entrained in the gyre system and flow northward. In contrast Site U1361 is under the influence of bergs generated along the George V Coast of the EAIS, which are entrained by the eastward flowing coastal counter current. During the Pliocene these bergs were locally sourced[26–28].

IODP Site U1524 is located ~120 km north of the Ross Sea continental shelf edge at 74°13.05′S, 173°37.98′W and in 2394 meters water depth (Fig. 1) on the crest of the levee adjacent to the Hillary Canyon submarine channel, the largest conduit for newly formed Antarctica Bottom Water (AABW) into the Pacific Ocean[31]. Sediment deposition at this site is influenced by the low-energy (non-erosive) suspension settling out of turbid spill-over from downslope cascading AABW. The transport of fine-grained muds and biogenic detritus from surface water plankton (i.e., diatoms) results in finely-laminated, diatom-rich muds and diatom oozes, superimposed with coarse sand and gravel deposited as IBRD (Fig. 2; see Supplementary Information for details on depositional setting)[32]. This succession provides an expanded Pliocene (3.3 to 2.6 Ma) interval and is the most continuous high-resolution record of this time interval recovered from the Antarctic continental margin (~20 cm/kyr). In Fig. 2 we plot time series of IBRD MARs, alongside paleoceanographic proxy data of biogenic opal MAR, and organic geochemical proxies (lipid biomarkers) for SST variability and meltwater input.

We assigned a downcore age scale via linear interpolation of a highly resolved bio-magnetostratigraphy correlated to the GPTS (geomagnetic polarity timescale)[32,33] (see Methods). Our datasets were not astronomically-tuned, or tied to the benthic $\delta^{18}O$ foraminifera record cycles, in order to avoid biases associated with proxy-based interpretation of globally-integrated ice volume change[34]. This avoidance of astronomical-tuning introduces some noise to our spectral analysis, particularly if there are large shifts in sedimentation rate that is unaccounted for by the coarser resolution bio-magnetostratigraphy (Supplementary Information). Our age model indicates an up-core decrease in sedimentation rate, associated with declining input of biogenic silica, but also indicates relatively continuous deposition that is not hindered by stratigraphic hiatuses as observed in the continental shelf AND-1B site[7] (Fig. 2). Notably, variability in sedimentation rates between paleomagnetic reversals, long-term shifts in sedimentation rate, and stochastic processes are not significant enough to distort a pure astronomical signal embedded within the Site U1524 record, thus providing additional confidence in our proxy times series results (Supplementary Information). Given that the WAIS is currently losing ice through iceberg discharge and supra- and sub-glacial melt processes[35,36], we interpret the variability embedded in our IBRD and meltwater-based proxies to reflect repetitive cycles of marine-based ice sheet mass change, that contributed to global sea level fluctuations with an amplitude of 5-25m during the mid-to Late Pliocene[12]. Our interpretation of the organic meltwater proxy (δD of *n*-C_{18}, see Methods) are consistent with freshwater dinoflagellate indicators (Supplementary Information).

Spectral analysis of the untuned Ross Sea IBRD MAR time series reveals statistically significant cycles that align with orbital frequencies associated with precession (~20-kyr), obliquity (~40-kyr), and eccentricity (~400 and ~100-kyr) (Fig. 4; Supplementary Information). The IBRD MAR signal is so robust that even with the addition of red noise to the data set, orbital frequencies are still statistically significant (Supplementary Information). Evolutive power spectral analysis demonstrates that between 3.4 and 2.8 Ma, strong and significant variance occurs within both eccentricity (~400 and ~100-kyr) and obliquity (~40-kyr) bands. However, after ~2.8 Ma the ~100-kyr eccentricity and 20-kyr precession signals dominate the record (Fig. 3). Untuned paleoceanographic proxy records in U1524 sediments for the mid-Pliocene interval between 3.3 to 3.0 Ma demonstrate that surface ocean productivity (Biogenic

Opal MAR) is significantly influenced by eccentricity and precession, whereas the δ_2H C_{18} fatty acid, an organic geochemical meltwater proxy, is primarily paced by obliquity (Fig. 2 and Supplementary Information).

We correlate cycles identified in the sedimentary proxies of Site U1524 with the cycles from a more proximal, but stratigraphically-less complete, Ross Sea geological record – ANDRILL AND-1B (Fig. 1 and 3). The latter captures WAIS grounding-line advance and retreat events on the continental shelf, as well as surface water conditions during interglacials[7,9]. Thus, we are able to link the direct evidence for obliquity-paced glacial-interglacial advance and retreat recorded at AND-1B[7] with the continuous high-resolution offshore record of iceberg rafting at Site U1524, in order to obtain a complete understanding of WAIS dynamics and associated oceanographic variability in the Ross Sea region.

West Antarctic Ice Sheet sensitivities to orbital forcing

Biogenic opal MAR and Natural Gamma Radiation (NGR) provide a measure of the relative abundance of diatom and terrigenous mud content (Fig. 2 and Supplementary Information). Within the mid-Pliocene Warm Period (mPWP) interval between 3.26-3.0 Ma (U1524, 270-200 m), low NGR and relatively high biogenic opal MAR values characterize a prolonged interval of diatom ooze deposition, that consists of highly fragmented frustules[32]. This interval is interpreted as reflecting highly-productive warm surface waters on the outer Ross Sea continental shelf - the source region for sediment passing down the Hillary Canyon and supplying deposition at the U1524 site. Low amplitude peaks in eccentricity and obliquity occur in the IBRD MAR throughout this interval, particularly when biogenic opal MAR values are relatively high. The high diatom-particulate burial flux in this interval (Fig. 2) suggests either an overall increase in surface water productivity during the warmer mid-Pliocene climate (3.3 to 3.0 Ma)[5,9], or a decrease in supply of glacimarine terrigenous sediment to the outer Ross Sea continental shelf. In either case, this increase in the biogenic component is interpreted to be a function of a distal AIS grounding line relative to the continental shelf break. This inferred reduction in the marine-based extent of West Antarctica is consistent with relatively lower IBRD MAR values compared to younger intervals. This interval correlates with the presence of mud-rich diatom facies in correlative interglacials in the AND-1B core associated with motif 2a. This interval in the AND-1B core is interpreted to represent a setting consistent with a southward retreat of the WAIS grounding and calving fronts in the Ross Sea sector compared with the Holocene, and an increased influence from surface-and basal melt processes. The significant precession (~20-kyr) signal identified in the biogenic opal MAR supports the notion that local, insolation-driven surface warming had a significant role in promoting the calving flux along this margin. However, the organic geochemical meltwater proxy reconstructions also demonstrate the significant role of surface-and or basal meltwater alongside calving fluxes in driving grounding line advance and retreat recorded in the lithological cycles of AND-1B[7] (Fig. 2).

While the IBRD MAR record appears to be strongly influenced by eccentricity and precession modulated changes in local insolation relating to surface melt processes in this interval (Fig. 2 & 3), the occurrence of obliquity in IBRD is consistent with rapid melt out and pulsing of icebergs from fast moving glaciers in the absence of an ice shelf[37] as they are exposed to an oceanic margin with sea surface temperatures (SST) of between 2 and 4°C[9] (Fig. 3). The Ross Sea records demonstrate that under the warmer climate regime of the mid-Pliocene, when local insolation is strong and sea ice extent along this margin is minimal, both atmospherically-driven surface warming modulated by eccentricity, and ocean-driven feedbacks associated with obliquity may contribute to WAIS ice volume changes reflected in the globally integrated benthic $\delta^{18}O$ LR04 ice volume record (Fig 3). However, the dominance of eccentricity and precession in far-field sea-level records[12,38] during this time implies a subordinate contribution of obliquity driven meltwater to global ice volume change.

After 3 Ma, the AND-1B record indicates that a cooling climate and ocean resulted in a decrease of outwash muds during interglacials that was interpreted as an increasing influence of iceberg calving processes on ice sheet mass balance (Fig. 2g)[9,39]. While the AND-1B record, contains an unconformity sometime between 2.9 to 2.7 Ma, the Site U1524 record supports this interpretation of shifting controls on WAIS mass balance, as there is an increased amplitude and shift in cyclicity associated with the IBRD

MAR record. Alongside this, NGR and MS values both increase, indicating of an increase in overall terrigenous input most likely related to an increase in erosional surface area along the shelf from more extensive periods of ice advance and a relative decrease in surface water productivity over the shelf break. Stratigraphically, the increased flux of IBRD within the middle of the Gauss subchron coincides with evidence in the ANDRILL-1B core of a transition in the WAIS to a polar style ice sheet with reduced meltwater influence[39], cooling SSTs (to ~1-2°C) and increased presence of perennial sea ice in the Ross Sea[7,9,39]. Consequently, the sedimentary packages in the AND-1B record indicate the development of larger marine-based ice sheets, and ice-shelves during some interglacials.

Twenty-thousand-year ice sheet model simulations starting with a 1000-year linear increase in atmospheric and ocean temperatures, initiated from present day conditions, demonstrate the relatively fast response in the percent change of grounded, and subsequently floating, ice in the WAIS Siple Coast and Amundsen Sea catchments. The loss of floating ice or ice shelves along the WAIS margin triggered by ocean-induced thinning and surface melt would have reduced buttressing and enhanced ice discharge and icebergs entering the into Southern Ocean (Supplementary Information). Notably, during the transition from the warmer 3.6-3 Ma climate recorded in the AND-1B record (Fig. 3), the obliquity signal in the IBRD record of Site U1524 is the strongest (Fig. 2). Thus, the data from U1524 and AND-1B, as well as model sensitivity tests demonstrate that the WAIS is inherently sensitive to all orbital forcing factors through atmospheric and marine driven processes, but the influence of those factors may change with time due to boundary conditions and warming scenarios. This may explain the disappearance of the significant obliquity signal after ~2.8 Ma in the Site U1524 record, although this signal reappears later in the Pleistocene in IBRD MAR records from the same margin[40].

Marine-based West and East Antarctic sensitivities to ocean and atmospheric forcing

The power spectra of IBRD MAR from WAIS (U1524) and EAIS (U1361) both demonstrate sensitivity to 100-kyr eccentricity modulation of local insolation from 3.3 to 2.3 Ma. Thus, WAIS and EAIS marine based margins in the Pacific Ocean sector were both sensitive to Southern Ocean or atmospheric feedbacks associated with austral summer insolation, controlled by precession and modulated by eccentricity[15,28,29]. However, the WAIS record deviates from the EAIS signature during the mid-Pliocene warm period from ~3.2 to 2.9 Ma, with a greatly enhanced sensitivity to obliquity- and precession- paced oscillations, which regulate changes in mean annual insolation and latitudinal temperature gradients. After ~2.9 to 2.75 Ma the reduction in obliquity coincides with an interpreted shift in the glacial regime, as inferred from the AND-1B record (Fig. 3). While the exact mechanistic influence that obliquity exerts on Pliocene AIS variability remains elusive[e.g., 7,23,41], it has recently been hypothesized that the ice sheet becomes most sensitive to obliquity forcing when it is grounded in a marine environment and when sea ice is limited during warm climates[10]. Consequently, we propose that obliquity amplifies wind-driven oceanic upwelling and basal melting processes that trigger ice sheet destabilization[18,19,42]. This is consistent with the pronounced precession signal in the astronomical solution during the warm mid-Pliocene compared to obliquity. When local insolation is most intense under a warm climate, only a small change in obliquity is required to amplify processes associated with, and driving, basal melt (Fig. 3).

While the Ross Sea sector of WAIS may have experienced an additional sensitivity to obliquity forcing when the coastal sea ice field was significantly reduced and the ice sheet extended into marine embayments during parts of the warm mid-Pliocene[7–9], the 100-kyr pacing throughout the mid-Pliocene to Early Pleistocene (3.3 to 2.3 Ma) in the Ross Sea sector of WAIS and along the marine-based EAIS Wilkes Land margin is consistent with large amplitude changes in sea level. These large amplitude changes require contributions from both marine-based WAIS and EAIS catchments (13 ± 5 m)[12,14,27,28,43] prior to the build-up of extensive ice sheets in North America (~2.7 Ma). Notably, the recently recovered geological records from IODP Expedition 382 in the Weddell Sea sector also demonstrates a significant eccentricity and precession pacing[16]. Relatively smaller coastal catchments along that margin may have experienced similar sensitives to atmospheric warming as the Wilkes Subglacial Basin along the George V coast[30] providing an additional contribution to sea level.

The lack of a significant obliquity pacing in the WAIS record after 2.75 Ma, and throughout most of the Wilkes Land EAIS record offshore the Wilkes Subglacial Basin, relative to the persistence of obliquity throughout LR04 record suggest the 41-kyr obliquity signal is primarily sourced from growth and decay of the Northern Hemisphere Ice Sheets (NHIS) (Fig. 3). Other ice sheet catchments around the AIS margin, such as the Recovery Basin of the EAIS in the Atlantic Ocean sector[30], could have been sensitivity to obliquity forcing. However, the Weddell Sea sector records do not demonstrate a strong and persistent obliquity signal until after ~2 Ma[16], similar to the Pleistocene Ross Sea IBRD MAR records[40]. Additionally, our modeling component highlights the longer response time of marine-based margins of EAIS compared to the WAIS for all potential warming scenarios.

In summary, we observe a non-linear response of marine-based Antarctic ice sheet catchments to natural temperature forcing mechanisms. This observation is supported by modeling that demonstrates a stronger sensitivity of the WAIS margin to oceanic forcing compared to EAIS during the warm mid-Pliocene. We conclude that if global mean temperatures exceed 2°C and sea ice conditions in the Ross Sea sector decrease, as analogous to the mid-Pliocene conditions, the Pacific Ocean sector of WAIS will undergo enhanced ocean-driven melt, consistent with modeling experiments.

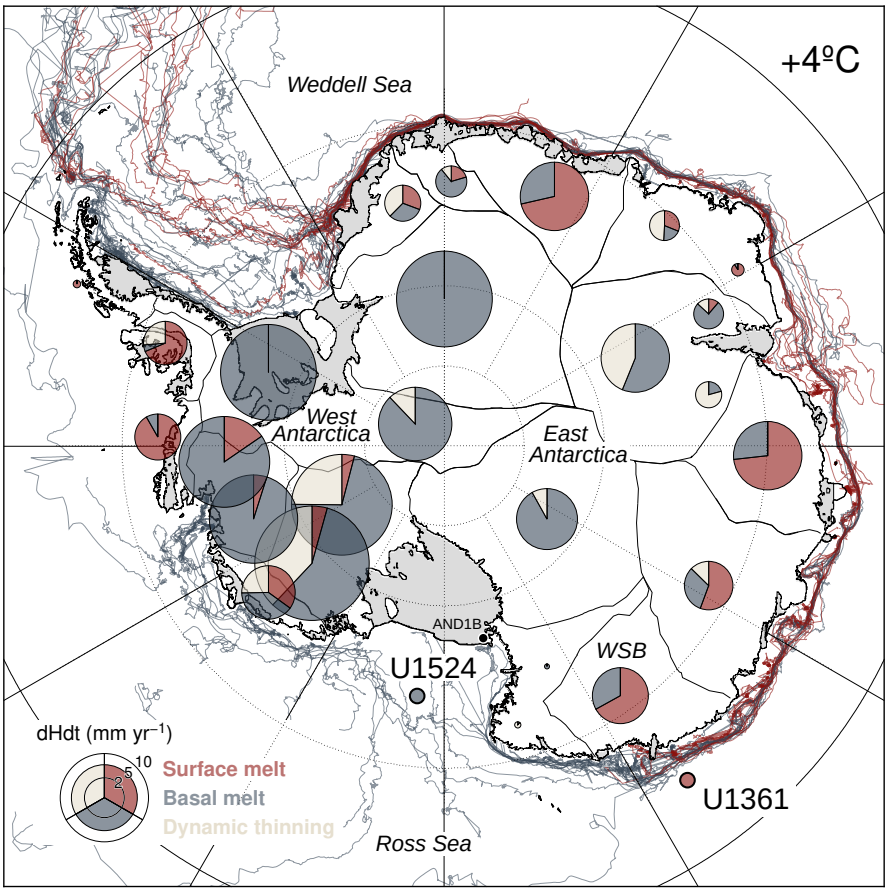

Figure 1. Location of IODP sites U1524 and U1361 and sources margin of icebergs tracked from 1978 & 1992 to 2021. The relative sensitivity of each Antarctic catchment to atmospheric forcing with a spatial uniform air temperature increase of 4°C. Ice mass loss through basal melt dominates West Antarctica catchments in the vicinity of U1524. Surface melt is the primary

process that contributes to ice mass loss associated with East Antarctic catchments associated with the Wilkes subglacial basin (WSB).

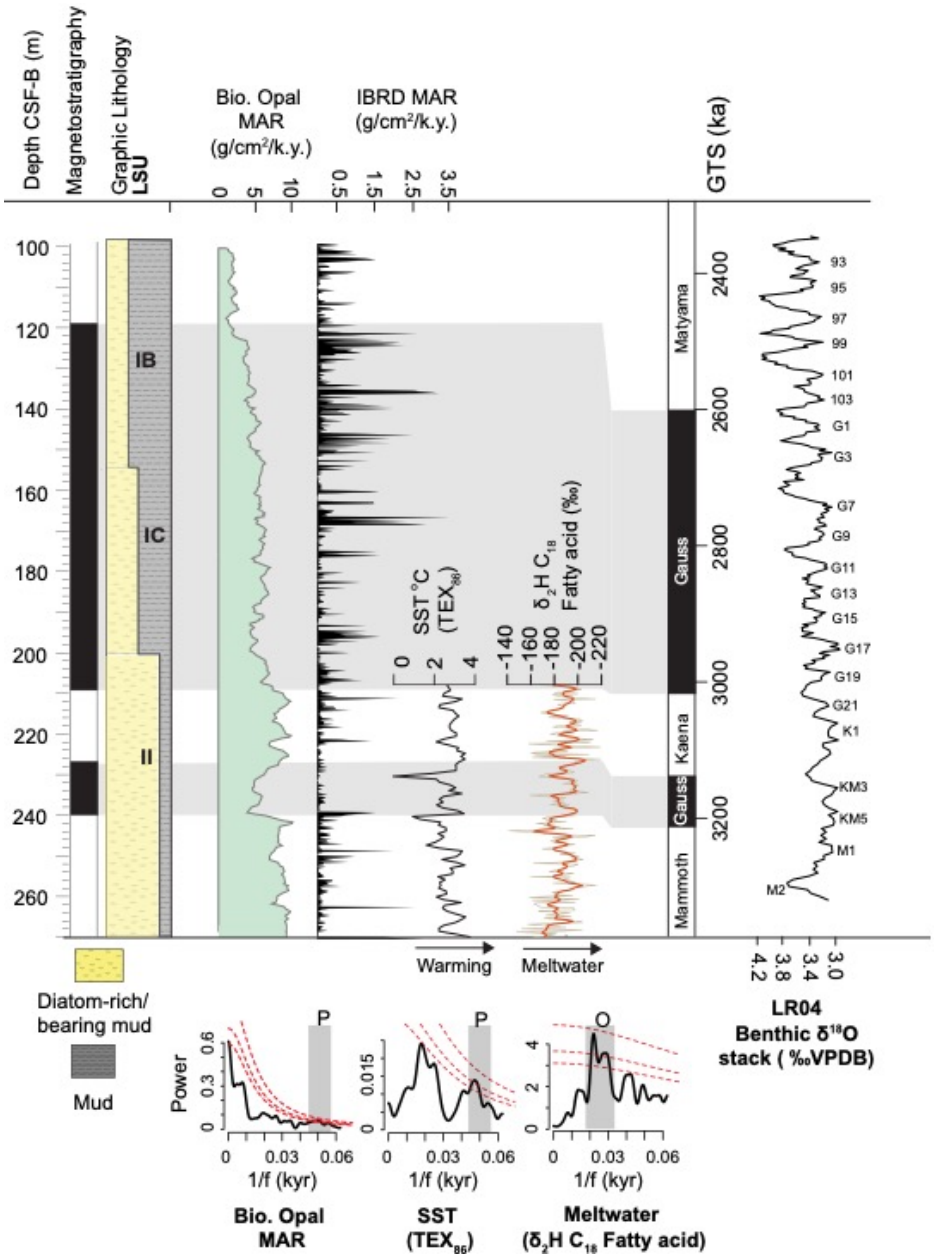

Figure 2. Depth series develop for IODP Site U1524 between 3.3 to 2.3 Ma. Stratigraphic and chronologic summary for the depth interval 270-100 m incudes: biogenic opal MAR, IBRD MAR, TEX_{86} derived SST (°C) estimates, and δ_2H C_{18} fatty acid record a proxy for meltwater are compared to the LR04 $\delta^{18}O$ stack[34]. Power spectral estimates for paleoceanographic proxies with significant precession (P) and obliquity (O) bands are highlighted in grey.

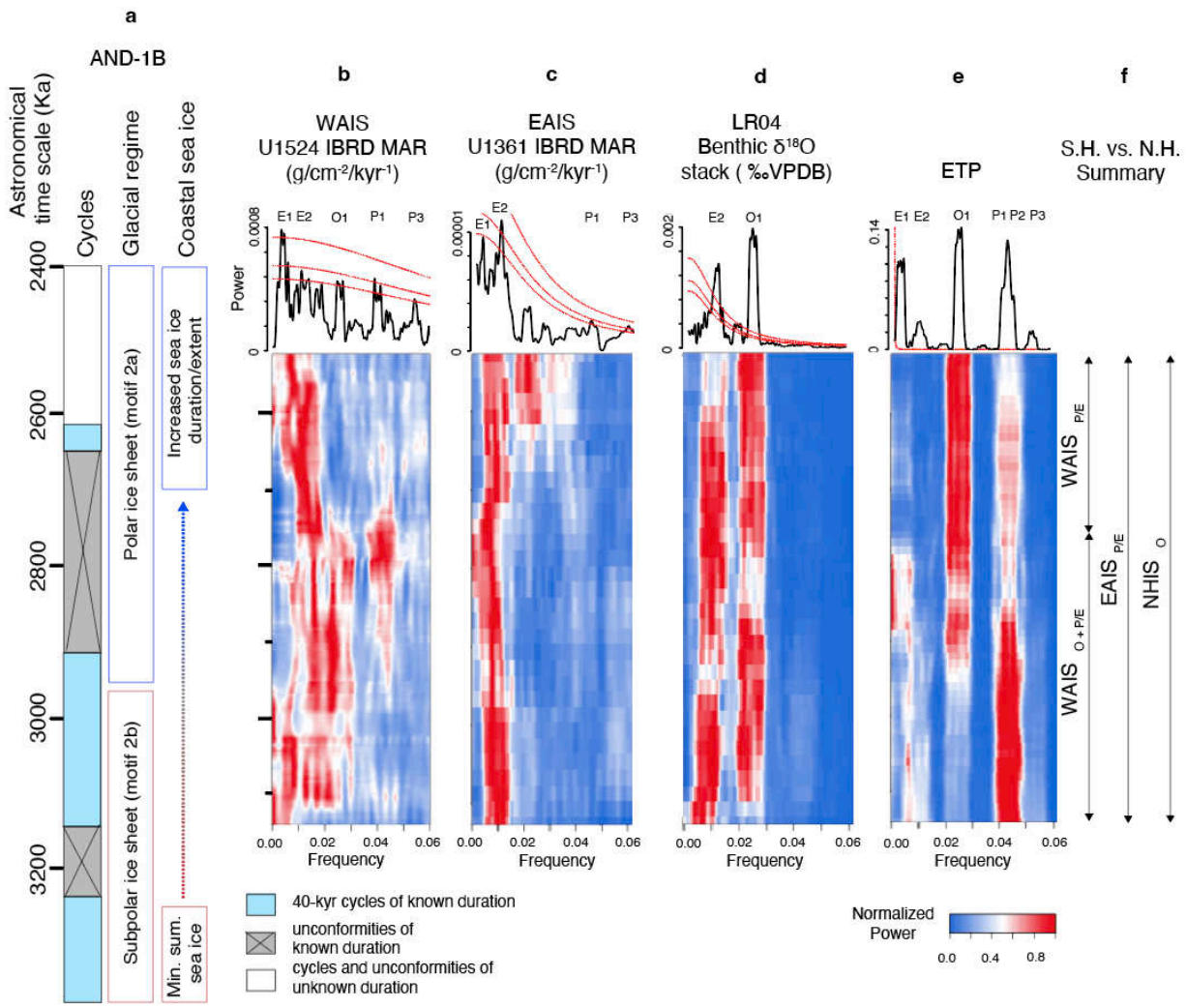

Figure 3. Power spectral estimates and multi-taper method time-frequency analysis (see Methods) of WAIS and EAIS IBRD MAR records and comparison with known obliquity paced 40-kyr glacial advance-retreat cycles, and the ice sheet-ocean-sea ice evolution in the Ross Embayment based on the AND-1B record (a)[7,9,39], the LR04 $\delta^{18}O$ stack(d)[34], and orbital parameters of eccentricity-tilt-precession (ETP)[45]. Power spectral estimates include significant orbital frequencies (e.g., E1, E2, O1, P1, P2, P3) identified in time series data (see Methods) and multi-taper method time-frequency analysis (see Methods) displays normalized power (colour scale) in **b-e**. Red dashed lines in power spectral estimates identify significance levels above 85%, 90% and 95% above confidence limits[46] respectively. **f**, summarizes Southern and Northern Hemisphere orbital forcing ice sheet scenarios discussed in this manuscript.

References

1. Intergovernmental Panel On Climate Change (Ipcc). *Climate Change 2021 – The Physical Science Basis: Working Group I Contribution to the Sixth Assessment Report of the Intergovernmental Panel on Climate Change*. (Cambridge University Press, 2023). doi:10.1017/9781009157896.

2. Martínez-Botí, M. A. *et al.* Plio-Pleistocene climate sensitivity evaluated using high-resolution CO2 records. *Nature* **518**, 49–54 (2015).
3. De La Vega, E., Chalk, T. B., Wilson, P. A., Bysani, R. P. & Foster, G. L. Atmospheric CO2 during the Mid-Piacenzian Warm Period and the M2 glaciation. *Sci. Rep.* **10**, 1–8 (2020).
4. Dowsett, H. J. *et al.* Assessing confidence in Pliocene sea surface temperatures to evaluate predictive models. *Nat. Clim. Change* **2**, 365–371 (2012).
5. Haywood, A. M. *et al.* Large-scale features of Pliocene climate: results from the Pliocene Model Intercomparison Project. *Clim. Past* **9**, 191–209 (2013).
6. Cenozoic CO2 Proxy Integration Project (CenCO2PIP) Consortium, et al. Toward a Cenozoic history of atmospheric CO2. *Science* **382**, 6675 (2023).
7. Naish, T. *et al.* Obliquity-paced Pliocene West Antarctic ice sheet oscillations. *Nature* **458**, 322 (2009).
8. Pollard, D. & DeConto, R. M. Modelling West Antarctic ice sheet growth and collapse through the past five million years. *Nature* **458**, 329–332 (2009).
9. McKay, R. *et al.* Antarctic and Southern Ocean influences on Late Pliocene global cooling. *Proc. Natl. Acad. Sci.* **109**, 6423–6428 (2012).
10. Levy, R. H. *et al.* Antarctic ice-sheet sensitivity to obliquity forcing enhanced through ocean connections. *Nat. Geosci.* **12**, 132–137 (2019).
11. Miller, K. G. *et al.* High tide of the warm Pliocene: Implications of global sea level for Antarctic deglaciation. *Geology* **40**, 407–410 (2012).
12. Grant, G. R. *et al.* The amplitude and origin of sea-level variability during the Pliocene epoch. *Nature* **574**, 237–241 (2019).
13. Williams, T. & Handwerger, D. A high-resolution record of early Miocene Antarctic glacial history from ODP Site 1165, Prydz Bay. *Paleoceanography* **20**, (2005).
14. Galeotti, S. *et al.* Antarctic Ice Sheet variability across the Eocene-Oligocene boundary climate transition. *Science* **352**, 76–80 (2016).

15. Patterson, M. O. *et al.* Orbital forcing of the East Antarctic ice sheet during the Pliocene and Early Pleistocene. *Nat. Geosci.* **7**, 841–847 (2014).
16. Reilly, B. T. *et al.* New Magnetostratigraphic Insights From Iceberg Alley on the Rhythms of Antarctic Climate During the Plio-Pleistocene. *Paleoceanogr. Paleoclimatology* **36**, e2020PA003994 (2021).
17. Timmermann, R. & Hellmer, H. H. Southern Ocean warming and increased ice shelf basal melting in the twenty-first and twenty-second centuries based on coupled ice-ocean finite-element modelling. *Ocean Dyn.* **63**, 1011–1026 (2013).
18. Toggweiler, J. R. & Russell, J. Ocean circulation in a warming climate. *Nature* **451**, 286–288 (2008).
19. Spence, P. *et al.* Rapid subsurface warming and circulation changes of Antarctic coastal waters by poleward shifting winds. *Geophys. Res. Lett.* **41**, 4601–4610 (2014).
20. Warm ocean is eroding West Antarctic Ice Sheet - Shepherd - 2004 - Geophysical Research Letters - Wiley Online Library. https://agupubs.onlinelibrary.wiley.com/doi/full/10.1029/2004GL021106.
21. Pattyn, F. & Morlighem, M. The uncertain future of the Antarctic Ice Sheet. *Science* **367**, 1331–1335 (2020).
22. DeConto, R. M. & Pollard, D. Contribution of Antarctica to past and future sea-level rise. *Nature* **531**, 591–597 (2016).
23. Huybers, P. Early Pleistocene Glacial Cycles and the Integrated Summer Insolation Forcing. *Science* **313**, 508–511 (2006).
24. The global influence of localized dynamics in the Southern Ocean | Nature. https://www.nature.com/articles/s41586-018-0182-3.
25. Wille, J. D. *et al.* Antarctic Atmospheric River Climatology and Precipitation Impacts. *J. Geophys. Res. Atmospheres* **126**, e2020JD033788 (2021).
26. Williams, T. *et al.* Evidence for iceberg armadas from East Antarctica in the Southern Ocean during the late Miocene and early Pliocene. *Earth Planet. Sci. Lett.* **290**, 351–361 (2010).

27. Cook, C. P. *et al.* Dynamic behaviour of the East Antarctic ice sheet during Pliocene warmth. *Nat. Geosci.* **6**, 765–769 (2013).
28. Bertram, R. A. *et al.* Pliocene deglacial event timelines and the biogeochemical response offshore Wilkes Subglacial Basin, East Antarctica. *Earth Planet. Sci. Lett.* **494**, 109–116 (2018).
29. Taylor-Silva, B. I. & Riesselman, C. R. Polar Frontal Migration in the Warm Late Pliocene: Diatom Evidence From the Wilkes Land Margin, East Antarctica. *Paleoceanogr. Paleoclimatology* **33**, 76–92 (2018).
30. Golledge, N. R., Levy, R. H., McKay, R. M. & Naish, T. R. East Antarctic ice sheet most vulnerable to Weddell Sea warming. *Geophys. Res. Lett.* **44**, 2343–2351 (2017).
31. Orsi, A. H. & Wiederwohl, C. L. A recount of Ross Sea waters. *Deep Sea Res. Part II Top. Stud. Oceanogr.* **56**, 778–795 (2009).
32. McKay, R. M., De Santis, L. & Kulhanek, D. K. Expedition 374 Preliminary Report: Ross Sea West Antarctic Ice Sheet History. *Prelim. Rep.* **374**, (2018).
33. Gradstein, F., Ogg, J. G., Schmitz, M. D. & Ogg, G. M. *The Geologic Time Scale 2012*. (Elsevier, 2012).
34. Lisiecki, L. E. & Raymo, M. E. A Pliocene-Pleistocene stack of 57 globally distributed benthic δ18O records. *Paleoceanography* **20**, (2005).
35. Depoorter, M. A. *et al.* Calving fluxes and basal melt rates of Antarctic ice shelves. *Nature* **502**, 89–92 (2013).
36. Paolo, F. S., Fricker, H. A. & Padman, L. Volume loss from Antarctic ice shelves is accelerating. *Science* **348**, 327–331 (2015).
37. Smith, J. A. *et al.* The marine geological imprint of Antarctic ice shelves. *Nat. Commun.* **10**, 5635 (2019).
38. Grant, G.R., & Naish, T.R. Pliocene sea level revisited: Is there more than meets the eye. *Past Global Changes Magazine* **29**.1, 34-35 (2021).

39. McKay, R. *et al.* The stratigraphic signature of the late Cenozoic Antarctic Ice Sheets in the Ross Embayment. *GSA Bull.* **121**, 1537–1561 (2009).
40. Ohneiser, C. *et al.* West Antarctic ice volume variability paced by obliquity until 400,000 years ago. *Nat. Geosci.* **16**, 44–49 (2023).
41. Raymo, M. E., Lisiecki, L. E. & Nisancioglu, K. H. Plio-Pleistocene Ice Volume, Antarctic Climate, and the Global δ18O Record. *Science* **313**, 492–495 (2006).
42. Schoof, C. Ice sheet grounding line dynamics: Steady states, stability, and hysteresis. *J. Geophys. Res. Earth Surf.* **112**, (2007).
43. Pollard, D., DeConto, R. M. & Alley, R. B. Potential Antarctic Ice Sheet retreat driven by hydrofracturing and ice cliff failure. *Earth Planet. Sci. Lett.* **412**, 112–121 (2015).
44. DeConto, R. M. & Pollard, D. Contribution of Antarctica to past and future sea-level rise. *Nature* **531**, 591 (2016).
45. Laskar, J., Fienga, A., Gastineau, M. & Manche, H. La2010: a new orbital solution for the long-term motion of the Earth. *Astron. Astrophys.* **532**, A89 (2011).

Methods

IBRD MAR

Six hundred and ninety samples of 20 cm^3 samples were freeze dried and wet sieved in order to determine the weight percent of the 250 μm to 2 mm fraction of coarse sand following the method of ref.[15]. The calculation of an Iceberg Rafted Debris Mass Accumulation Rate (IBRD MAR) of the coarse sand fraction was estimated using the following equation:

$$\text{IBRD MAR} = \text{CS\%} * \text{DBD} * \text{LSR},$$

where IBRD MAR is the mass accumulation rate ($g/cm^2/k.y.$), CS% is the coarse-sand weight percent, DBD is the dry-bulk density of the "nearest" value (g/cm^3) and LSR is the sampled interval average linear sedimentation rate (cm/k.y.).

Biogenic opal (Oscar)

Biogenic silica (opal) was measured using a sequential leaching technique in the MARUM Opallab (University of Bremen, Bremen, Germany)[47]. The precision of the sequential leaching technique is better than 0.5%[47]. The spatial resolution of bSi measurements were taken every 40 cm. The precision of the overall method based on replicate analyses is mostly between ± 0.2 and ± 0.4%, depending on the composition of the material analyzed. For standard deviations of

biogenic silica measurements, we refer to[47]. For the interval 3.31-2.42 Ma, biogenic silica ranges 5.39 and 75.0wt.% (average $29.70 \pm 11.06 wt.\%$).

Palynology (Fran)

Sample processing was performed at Utrecht University, following standard techniques of the Laboratory of Palaeobotany and Palynology. Samples were oven-dried and weighed (~15 g dry weight sediment each). One Lycopodium clavatum tablet with a known amount of marker spores was added for quantification of palynomorph abundances[48].

Samples were treated with 10% HCl (Hydrochloric acid) and cold 38% HF (Hydrofluoric acid), then sieved over a 10 µm mesh with occasional mild ultrasonic treatment. To avoid any potential processing-related preservation bias, no oxidation or acetolysis was carried out. The processed residue was transferred to microscope slides using glycerine jelly as a mounting medium, and 2 slides were analysed per sample at 400× magnification. Slides were examined for detailed marine palynomorphs (dinoflagellate cysts, acritarchs and other aquatic palynomorphs). Dinocysts were identified based on a taxonomical index[49] and informally and formally described species in the literature[50,51]. Dinocyst percentages were calculated based on the total in situ dinocysts counted, excluding reworked specimens. Reworked dinocysts include few specimens or fragments of Eocene and Oligocene taxa (mostly Vozzhennikovia spp.). In situ dinocyst and other palynomorphs like the brackish water algae Cymatiosphaera spp. absolute abundance (specimens/g dry weight) were calculated by counting the amount of Lycopodium clavatum spores encountered, following the equation of ref.[52].

Organic Geochemical proxies (Osamu)

Lipid compounds were extracted from homogenized dry sediment with Dionex-ASE200. Total extracts were separated into neutral and acid fractions by aminopropyl silica gel column chromatography[53]. The acid fraction was methylated by using methanol–acetyl chloride, and then purified with silica gel column chromatography. δD (‰, vSMOW) of *n*-C_{18} fatty acid methyl esters was measured using a gas chromatograph-thermal conversion-isotope ratio mass spectrometry (GC-TC-IRMS) system consisting of HP7890 GC, thermal conversion interface and an Elementar isoprime visION mass spectrometer. The measured δD value of *n*-C_{18} fatty acid methyl esters was corrected by an isotopic mass balance equation for the contribution of hydrogen added during esterification.

The neutral fraction was further separated into subfraction for glycerol dialkyl glycerol tetraether (GDGT) analysis. GDGTs were analyzed using high performance liquid chromatography-mass spectrometry (HPLC-MS) with an Agilent 1260 HPLC system coupled to 6130 quadrupole mass spectrometer. The standard deviations of crenarchaeol, GDGT-I, GDGT-II and GDGT-III measurements in replicate LC/MS analysis were 1, 1, 3 and 2% in sediment samples, respectively. TEX_{86}^{L} index was converted into temperature using ref.[54] equation: $T = 50.8 \times TEX_{86}^{L} + 36.1$.

Age model

The age model consists of a highly resolved magnetostratigraphy (average sample spacing = ~0.6 m; 3 kyr resolution for the Pliocene; 13 kyr resolution for the Pleistocene) guided by well-constrained age-diagnostic biostratigraphic events, and is correlated to the GPTS (geomagnetic polarity timescale)[32,33]. The error surrounding paleomagnetic reversals is on average of ~1.0 m or ~5.6 kyr, based on linear sedimentation rates within each chron/subchron

and spacing of discrete paleomagnetic samples. This error is an order of magnitude less than the error in another published Antarctic ice marginal record from a similar setting, IODP Site U1361, along the Wilkes Land margin, where orbital scale variability of the ice sheet was quantified[15,55].

Time series analysis

Time series analysis for this study used "Astrochron: An R package for Astrochronology"[56]. Prior to analysis all data was resampled at a median sample resolution or greater and detrended. All power spectral analysis used the multitaper method (MTM)[57], with three 2π prolate tapers and identified significant orbital frequencies using three red noise confidence level estimates[46,57,58], based on the orbital solution of ref.[45]. Time-frequency MTM analysis included a 450-kyr window at a time-step equal to or greater to the sample resolution. Each window was linearly detrended before analysis. All code is available as Supplementary Information.

Ice Sheet Modeling

To objectively investigate the differing responses of West and East Antarctic ice sheet catchments and to quantify their respective behaviours we use an ensemble of ice sheet model experiments that capture a broad range of possible climate (ocean and atmosphere) scenarios[30]. Our simulations use the Parallel Ice Sheet Model version 0.6.3[59,60], a fixed-grid hybrid ice flow model that superposes velocity solutions from both the shallow ice (SIA), and the shallow shelf (SSA), approximations of the Navier-Stokes flow equations. This hybrid scheme allows for a spatially consistent representation of flow by internal deformation (creep) and by longitudinal stretching, enabling dynamically diverse regions such as the slow-flowing ice sheet interior as well as faster-flowing outlet glaciers, ice streams, and fully-floating shelf ice to be captured in a contiguous manner. Basal sliding of grounded ice occurs in an entirely emergent way depending on the thermal state of the basal ice and the yield strength of subglacial sediments. This latter term is initialised from an elevation-dependent piecewise-linear prescription of till friction angle, such that deeper beds are given lower friction values in recognition of their greater likelihood of containing soft (potentially marine) sediments. Higher elevation topography is assigned higher friction, on the assumption that sediment cover may be less, and bare bedrock may be more common. Pore water arising from basal melting of ice is allowed to permeate the substrate and in doing so reduces its yield strength. Cyclic oscillations may therefore arise in which thickening ice leads to greater basal melt that triggers sliding, which in turn thins the ice, reducing basal melt and sliding, and allowing renewed thickening[61,62].

To accurately track the changing position of the junction between grounded and floating ice we employ a grounding-line scheme that uses a subgrid interpolation[63]. This scheme as implemented in these experiments interpolates basal driving stress across the grounded-floating transition but is not used to interpolate basal melting, meaning that sub-ice shelf melt rates are only applied to fully floating cells and do not extend landward. Bed deformation due to ice loading is accounted for following the fast-Fourier transform model of[64], which accurately captures the multi-millennial scale viscous deformation of the mantle relevant to the orbital timescales of our study. Melting at the base of ice shelves (and at the grounding line) is calculated from a three-equation model[65,66] that determines the freezing point in the boundary layer from prescribed spatial fields of ocean temperature, salinity, and depth.

To enable computational tractability of our ensemble of 42 x 20,000 year-long simulations we employ a spatial grid size of 20 km. Our experiments all start from a present-day ice sheet configuration that is close to a steady state, using air temperatures from ref.[67] and a surface mass balance field from ref.[68]. The model is run for 2000 years under these (constant) conditions, followed by a 1000-year-long linear increase in both oceanic and atmospheric temperatures that is then held constant for the remainder of the run. Temperature anomalies are applied in a spatially uniform manner. Perturbed atmospheric temperatures are linked to precipitation, such that the latter increases by 5.3% for each degree of atmospheric warming, in line with observations and models[69]. Further information on the model used and previous implementations can be found elsewhere[30,70].

Data availability

Data and scripts will be made available as supplementary information during time of publication.

Acknowledgements

This research used data and samples provided by the International Ocean Discovery Program (IODP), which is sponsored by the US National Science Foundation (NSF) and participating countries under the management of Joint Oceanographic Institutions. Development of the IBRD MAR record was funded by grant numbers NSF-OCE 1450528 and NSF-OPP 2000997. Organic geochemical palaeoceanographic proxies (TEX_{86}^{L} and δD of *n*-C_{18} fatty acid) performed by O.S. and M.Y. was funded by the Japan Society for the Promotion of Science (JSPS) KAKENHI Grant Numbers 17H01166, 17H06318, and 20H00626. Biogenic opal MAR was determined by O.E. R. and funded by the German Research Foundation (DFG) (R03039/4). NRG was funded by the Royal Society of New Zealand contract VUW-1501 and by Ministry for Business, Innovation and Employment contracts RTUV1705 (NZSeaRise). RM was funded by Royal Society of New Zealand Marsden Fund contract MFP-VUW2207. RM and NRG were supported by ANTA1801 (Antarctic Science Platform). PISM is supported by NASA grant numbers NNX13AM16G and NNX13AK27G. T.E.v.P. was supported as Research Fellow by the University of Leicester and NERC NE/R018235/1. We also thank the numerous scientists who collected site survey data and developed the proposals and hypotheses that led to IODP Expedition 374. Expedition 374 was conducted under Antarctic Conservative Act Permit Number: ACA 2018-027 (permit holder: Bradford Clement, JRSO, IODP, TAMU, College Station, TX 77845).

Author contributions

M.O.P., C.R., O.S., O.E.R., M.N., F.S., R.M., G.G., and N.R.G. designed the research in collaboration with the entire IODP expedition 374 science party. C.R. produced U1524 IBRD MAR record. O.S. carried out all organic geochemical analysis and produced the TEX_{86} and δ_2H C_{18} fatty acid data sets. O.R. collected biogenic opal data. M.N. and F.S. collected palynology data. N.G. carried out ice sheet modeling experiments. Time series analysis was carried out by M.O.P., W.D.A., and H.J. in collaboration with S.M. Age model development was carried out by G.C., D.H., D.K., R.M.L., O.R., S.T.S., T.v.P., and W.X. Sedimentological interpretations were made by M.O.P., J.A., I.C.D., S.I., B.K., S.K., S.L., A.S., and S.S. Physical property data sets were developed by B.R., F.B., I.B., J.G., and S.K. Figure 1 was created by N.R.G. Figure 2 and 3 were created by G.G. and M.O.P. R.M., G.G., B.K., T.N., R.L., S.M., N.S., and N.V. assisted in interpretations of the data. All authors contributed to drafting the manuscript. R.M. and L.D.

were co-chiefs of IODP Expedition 374. All IODP Expedition 374 scientists contributed to the collection of shipboard datasets and initial interpretations for Site U1524.

Supplementary Information is available for this paper.

The authors declare no competing interests.

Correspondence and requests for materials should be addressed to Molly O. Patterson.

Method References

46. Mann, M. E. & Lees, J. M. Robust estimation of background noise and signal detection in climatic time series. *Clim. Change* **33**, 409–445 (1996).

47. Müller, P. J. & Schneider, R. An automated leaching method for the determination of opal in sediments and particulate matter. *Deep Sea Res. Part Oceanogr. Res. Pap.* **40**, 425–444 (1993).

48. Chapter 3. Palynological techniques-processing and microscopy. In. Jasonius, J. and McGregor, D. C. eds., Palynology: Principles and Application. | CiNii Research. https://cir.nii.ac.jp/crid/1572543024138151168.

49. Lentin, J. K. & Williams, G. L. *Fossil Dinoflagellates: Index to Genera and Species*. vol. 20 (American Association of Stratigraphic Palynologists Foundation, 1989).

50. Clowes, C. D., Hannah, M. J., Wilson, G. J. & Wrenn, J. H. Marine palynostratigraphy and new species from the Cape Roberts drill-holes, Victoria land basin, Antarctica. *Mar. Micropaleontol.* **126**, 65–84 (2016).

51. Bijl, P. K., Houben, A. J. P., Bruls, A., Pross, J. & Sangiorgi, F. Stratigraphic calibration of Oligocene–Miocene organic-walled dinoflagellate cysts from offshore Wilkes Land, East Antarctica, and a zonation proposal. *J. Micropalaeontology* **37**, 105–138 (2018).

52. Benninghoff, W. S. *Calculation of Pollen and Spore Density in Sediments by Addition of Exotic Pollen in Known Quantities*. (1962).

53. Gao, L., Guimond, J., Thomas, E. & Huang, Y. Major trends in leaf wax abundance, δ2H and δ13C values along leaf venation in five species of C3 plants: Physiological and geochemical implications. *Org. Geochem.* **78**, 144–152 (2015).
54. Holocene subsurface temperature variability in the eastern Antarctic continental margin - Kim - 2012 - Geophysical Research Letters - Wiley Online Library. https://agupubs.onlinelibrary.wiley.com/doi/full/10.1029/2012GL051157.
55. Tauxe, L. *et al.* Chronostratigraphic framework for the IODP Expedition 318 cores from the Wilkes Land Margin: Constraints for paleoceanographic reconstruction. *Paleoceanography* **27**, (2012).
56. astrochron: A Computational Tool for Astrochronology.
57. Thomson, D. J. Spectrum estimation and harmonic analysis. *Proc. IEEE* **70**, 1055–1096 (1982).
58. Meyers, S. R. Seeing red in cyclic stratigraphy: Spectral noise estimation for astrochronology. *Paleoceanography* **27**, 2012PA002307 (2012).
59. Bueler, E. & Brown, J. Shallow shelf approximation as a "sliding law" in a thermomechanically coupled ice sheet model. *J. Geophys. Res. Earth Surf.* **114**, 2008JF001179 (2009).
60. Winkelmann, R. *et al.* The Potsdam parallel ice sheet model (PISM-PIK)–Part 1: Model description. *The Cryosphere* **5**, 715–726 (2011).
61. Van Pelt, W. J. & Oerlemans, J. Numerical simulations of cyclic behaviour in the Parallel Ice Sheet Model (PISM). *J. Glaciol.* **58**, 347–360 (2012).
62. Golledge, N. R. *et al.* Antarctic contribution to meltwater pulse 1A from reduced Southern Ocean overturning. *Nat. Commun.* **5**, 5107 (2014).
63. Feldmann, J., Albrecht, T., Khroulev, C., Pattyn, F. & Levermann, A. Resolution-dependent performance of grounding line motion in a shallow model compared with a full-Stokes model according to the MISMIP3d intercomparison. *J. Glaciol.* **60**, 353–360 (2014).
64. Bueler, E. D., Lingle, C. S. & Brown, J. Fast computation of a viscoelastic deformable Earth model for ice-sheet simulations. *Ann. Glaciol.* **46**, 97–105 (2007).

65. Hellmer, H., Jacobs, S. S. & Jenkins, A. Oceanic erosion of a floating Antarctic glacier in the Amundsen Sea. *Ocean Ice Atmosphere Interact. Antarct. Cont. Margin Jacobs R Weiss Eds Antarct. Res. Ser. AGU Wash. DC USA* **75**, 319–339 (1998).
66. Holland, D. M. & Jenkins, A. Modeling thermodynamic ice–ocean interactions at the base of an ice shelf. *J. Phys. Oceanogr.* **29**, 1787–1800 (1999).
67. Comiso, J. C. Variability and trends in Antarctic surface temperatures from in situ and satellite infrared measurements. *J. Clim.* **13**, 1674–1696 (2000).
68. Lenaerts, J. T. M., Van Den Broeke, M. R., Van De Berg, W. J., Van Meijgaard, E. & Kuipers Munneke, P. A new, high-resolution surface mass balance map of Antarctica (1979–2010) based on regional atmospheric climate modeling. *Geophys. Res. Lett.* **39**, 2011GL050713 (2012).
69. Frieler, K. *et al.* Consistent evidence of increasing Antarctic accumulation with warming. *Nat. Clim. Change* **5**, 348–352 (2015).
70. Golledge, N. R. *et al.* Antarctic climate and ice-sheet configuration during the early Pliocene interglacial at 4.23 Ma. *Clim. Past* **13**, 959–975 (2017).

Supplementary Files

This is a list of supplementary files associated with this preprint. Click to download.

- Pattersonetal.SupplementaryMaterial.docx
- pattersonetal2024supplemental.txt